

Article

Fundamental Understanding of Dye Coverage and Performance in Dye-Sensitized Solar Cells Using Copper Electrolyte

Sourava Chandra Pradhan ^{1,2}, Jayadev Velore ^{1,2}, Sruthi Meledath Meethal ^{1,2} and Suraj Soman ^{1,2,*} 

¹ Centre for Sustainable Energy Technologies (C-SET), CSIR-National Institute for Interdisciplinary Science and Technology (CSIR-NIIST), Thiruvananthapuram 695019, India

² Academy of Scientific and Innovative Research (AcSIR), Ghaziabad 201002, India

* Correspondence: suraj@niist.res.in

Abstract: Dyes have played a pivotal role in the advancement of modern dye-sensitized solar cells (DSCs), as they not only facilitate light harvesting, but also serve as blocking layers to impede recombination. In this study, we conducted a systematic investigation to elucidate the influence of dye coverage on the photovoltaic parameters of copper-electrolyte-based DSCs by precisely controlling the dye coverage on the TiO₂ substrate using D35 organic dye solutions with varying concentrations. The dye loading increased proportionally with the increase in dye concentrations until it reached saturation at a concentration of 0.2 mM. However, an optimal dye concentration of 0.1 mM was determined in terms of achieving the highest photovoltaic performance, under both outdoor and indoor light conditions. Notably, a maximum power conversion efficiency (PCE) of $6.50 \pm 0.25\%$ under outdoor illumination (100 mW/cm²) and $10.48 \pm 0.30\%$ under indoor light (1000 lux, WW CFL) was attained using a 0.1 mM D35 dye concentration. Additionally, the dark current and ideality factor (*m*) were found to be minimized at the 0.1 mM dye concentration. Furthermore, the ideality factor (*m*) exhibited disparities between indoor and outdoor light conditions. The lifetime obtained from electrochemical impedance spectroscopy (EIS) measurements correlated well with the ideality factor (*m*) and dark current. Notably, electron injection, dye regeneration, charge collection, and ion diffusion were observed to be independent of the dye coverage.

Keywords: copper electrolyte; dye; DSC; indoor photovoltaics



Citation: Pradhan, S.C.; Velore, J.; Meethal, S.M.; Soman, S. Fundamental Understanding of Dye Coverage and Performance in Dye-Sensitized Solar Cells Using Copper Electrolyte. *Energies* **2023**, *16*, 6913. <https://doi.org/10.3390/en16196913>

Academic Editors: Yasemin Saygili and Audun Formo Buene

Received: 25 June 2023

Revised: 6 August 2023

Accepted: 11 August 2023

Published: 30 September 2023



Copyright: © 2023 by the authors. Licensee MDPI, Basel, Switzerland. This article is an open access article distributed under the terms and conditions of the Creative Commons Attribution (CC BY) license (<https://creativecommons.org/licenses/by/4.0/>).

1. Introduction

Dye-sensitized solar cells (DSCs) are considered to be among the most promising cost-effective and environmentally friendly photovoltaic technologies [1–3]. DSCs are endowed with many striking features such as color tunability, transparency, flexibility, and superior performance under indoor/artificial illumination, which makes them attractive for the development of self-powered, battery-free smart devices [2,4–7]. During the last three decades, DSCs have significantly transformed to a stage capable of realizing market penetration. Modern DSCs are among the few technologies that work efficiently under indoor/ambient light conditions with PCE > 30% and are now commercialized by many industries globally as energy sources for various Internet of Things (IoT)-based electronic devices [8–10]. Furthermore, they have also started to establish a presence in the building-integrated photovoltaic (BIPV) sector [11–15].

Unlike conventional DSCs, which consist of ruthenium metal complex sensitizers and iodide/triiodide (I^-/I_3^-) redox mediators, modern DSCs rely on organic dyes with alternate transition metal complex redox mediators ($Co^{3+/2+}/Cu^{2+/1+}$) [16–19]. Alternate redox mediators render an opportunity to modify the redox potential, thereby minimizing voltage loss and leading to higher open circuit potential (V_{oc}). Likewise, organic sensitizers possess a higher molar extinction coefficient, which helps in better light-harvesting properties, contributing towards improved J_{sc} using thin TiO₂ layers. The combination

of organic dyes and alternate electrolytes generates enormous opportunities to fine-tune the device properties and to meet the end-user requirements [20,21]. For instance, recently Naim et al. successfully achieved fully transparent DSCs using a selective near-infrared sensitizer based on a polymethine cyanine dye along with a cobalt redox mediator [22]. Similarly, Hualme et al. were able to fabricate photochromic DSCs that can change color with self-adjustable light transmittance when irradiated [23]. Moreover, presently DSCs have already reached an efficiency of 15.2% using co-sensitized organic dyes (SL9 and SL10) along with a copper electrolyte ($[\text{Cu}(\text{tmby})_2]^{2+/1+}$) under outdoor/one sun illumination (AM 1.5 G, 100 mWcm^{-2}) [24]. Similarly, an impressive power conversion efficiency of 34.5% has already been achieved using a co-sensitized XY1+MS5 dye combination along with a $[\text{Cu}(\text{tmby})_2]^{2+/1+}$ electrolyte under 1000 lux CFL illumination [8]. Earth-abundant copper redox mediators have played a significant role in the evolution of modern DSCs, particularly for indoor photovoltaics (IPVs) [9,16,25–27]. Copper redox shuttles are cost-effective and environmentally friendly, thus possessing adequate potential for industrialization and mass production. More importantly, copper-based redox mediators can sufficiently regenerate the oxidized dye molecules with efficiencies close to unity, even with a driving force as low as 0.1 V [28–30]. Using $\text{Cu}^{\text{II/I}}$ redox couples, $V_{\text{oc}} > 1 \text{ V}$ can easily be obtained without compromising J_{sc} . Recently, our research group has successfully attained an impressive open-circuit voltage (V_{oc}) of 1.27 V in a single-junction device, employing the $[\text{Cu}(\text{dmp})_2]^{2+/1+}$ redox mediator in combination with the MS5 dye [31]. In classical DSCs, dye is responsible for the current generation through light absorption; however, in modern DSCs, the role of the dye is not merely limited to light absorption—it also plays a pivotal role in preventing recombination at the TiO_2 -electrolyte interface [32–35]. For instance, Tang et al. effectively regulated charge recombination by increasing the dye concentration, which helped them to obtain high FF even in TiO_2 with a thickness of 20 μM [36]. Similarly, Pazoki et al. carried out a detailed analysis of dye coverage on charge recombination in a DSC with a cobalt tris(bipyridine) electrolyte and the D35 dye, where they found that more than 90% of full dye coverage is needed for well-performing DSCs with a cobalt-based electrolyte [37]. When employing alternate redox mediators like copper complexes with positive redox potentials, recombination is a critical issue. Furthermore, under low indoor/artificial light illuminations, recombination becomes essentially more crucial, where even a small increase in recombination can subsequently hamper the efficiency in a bigger way. Addressing recombination using additional blocking layers has already proven to be an efficient and conventional method, but it possesses several bottlenecks in scaling-up. Thus, modifying the dye coverage on TiO_2 and thereby controlling recombination offers a better possibility to achieve higher V_{oc} and PCE. To enhance our knowledge on the fundamental understanding of various charge-transfer processes as a function of dye coverage using a copper redox mediator, D35 organic dye in different concentrations was used to control the dye loading on TiO_2 and we systematically investigated its effect on the PV parameters using a $[\text{Cu}(\text{tmby})_2]^{2+/1+}$ electrolyte both under one-sun (AM 1.5 G, 100 mW/cm^2) and indoor illumination (1000 lux, WW CFL).

2. Materials and Methods

For the working electrode, $1.5 \times 1.5 \text{ cm}^2$ square FTO (TEC15, Greatcell Solar, Queanbeyan, NSW, Australia) substrates underwent a rigorous cleaning process, starting with sonication in detergent for 30 min and gentle scrubbing in water. Subsequently, they were sonicated in deionized (DI) water for another 30 min, followed by sonication in both IPA and acetone for 15 min each. Next, the FTO substrates were annealed at $500 \text{ }^\circ\text{C}$ for 15 min in a muffle furnace and then subjected to UV-ozone cleaning. A compact TiO_2 blocking layer over the FTO was deposited by TiCl_4 treatment and annealing at $500 \text{ }^\circ\text{C}$ for 30 min. This treatment involved dipping cleaned FTO substrates in a 53 mM TiCl_4 bath at $70 \text{ }^\circ\text{C}$, followed by rinsing with DI water and ethanol. A TiO_2 paste containing 30 nm particles was screen-printed onto the substrate and annealed at $500 \text{ }^\circ\text{C}$ for 30 min. Subsequently, a second TiCl_4 treatment was applied to the electrodes, followed by annealing at $500 \text{ }^\circ\text{C}$

for 30 min to create a compact TiO₂ post-blocking layer over the mesoporous TiO₂. For dye loading, the electrodes were then immersed in the D35 dye bath for 15 h. The dye solution was prepared using a 1:1 mixture of acetonitrile and tert-butanol. For counter electrodes, predrilled FTO glasses (TEC8, Greatcell Solar, Queanbeyan, NSW, Australia) were thoroughly cleaned by sonication in detergent, DI water, and ethanol for 45 min, followed by annealing at 500 °C for 15 min. Prior to PEDOT (poly (3,4-ethylene dioxythiophene)) deposition, the electrodes were treated with UV-O₃ for 15 min. The PEDOT counter electrodes were prepared by electro polymerization of 3,4-ethylene dioxythiophene (EDOT) from a micellar aqueous solution containing 0.1 M sodium dodecyl sulfate (SDS) and 0.01 M EDOT. The electrodes were assembled using a 25 µm surlyn spacer and heat pressed at 110 °C [38–40]. [Cu(tmby)₂]^{2+/1+} electrolyte, consisting of 0.20 M Cu(I), 0.04 M Cu(II), 0.1 M LiTFSI, and 0.6 M 4-tert-butylpyridine in acetonitrile was injected through the predrilled holes, and then the holes were sealed using a cover glass.

Solar photocurrent density voltage (J-V) characteristics of the DSCs were evaluated using the Oriel Class-AAA solar simulator (Model PVIV-94043A) in conjunction with the Keithley 2440 power source. The intensity of irradiation was measured using a certified calibrated Si solar cell. Indoor light photovoltaic measurements of DSCs were conducted inside a dark box, utilizing a worm white compact fluorescent lamp (WWCFL) as the illumination source. The indoor J-V responses of the DSCs were recorded using a Dyenamo (Stockholm, Sweden) potentiostat (DN-AE05), enabling precise data acquisition. To quantify the intensity of the light, a radiometrically calibrated spectrometer (Jaz, Ocean Optics, Orlando, FL, USA) was employed, ensuring accurate and reliable measurements of the light spectrum. During the J-V measurements DSCs, a circular black mask with an area of 0.12 cm² (smaller than the active area) was employed. The incident photon-to-current conversion efficiency (IPCE) measurements of the DSCs were conducted in DC mode using dedicated IPCE equipment. The setup consisted of a 300 W Xenon lamp integrated with a Newport (USA) monochromator and power meter. For Electrochemical Impedance Spectroscopy (EIS) analysis, the DSCs were tested under dark conditions using an Autolab (PGSTAT302N) system from the Netherlands. EIS was performed with an amplitude perturbation of 10 mV and a frequency range from 100 mHz to 100 kHz. Photo-induced absorption spectroscopy (PIA) was carried out using PIA equipment from Dyenamo, Sweden (DN-AE02). The PIA spectra of the devices were recorded using excitation by LED, which has a square wave with a modulation frequency of 9.3 Hz.

3. Results

3.1. Solar Cell Characteristics under Outdoor and Indoor Light

For the photovoltaic studies, we fabricated DSCs employing an organic D35 dye along with a [Cu(tmby)₂]^{2+/1+} redox mediator. Figure 1a shows the structure of the D35 dye and [Cu(tmby)₂]^{2+/1+} redox mediator. As shown in Figure 1b, the D35 dye and [Cu(tmby)₂]^{2+/1+} redox mediator possess favorable energetics for efficient charge injecting and dye regeneration. The D35 dye was selected for the present study as it is free from dye aggregation, providing a platform to exclusively study the charge recombination at the TiO₂/electrolyte interface [41,42]. We quantified the amount of dye on TiO₂ via a desorption study (Figure 1c). In all fabricated DSCs, TiO₂ photoanodes with a thickness of 4 µm and dye loading time of 15 h were used. As observed in Figure 1c, dye loading improved with an increase in dye concentration and reached a saturation at 0.2 mM dye concentration.

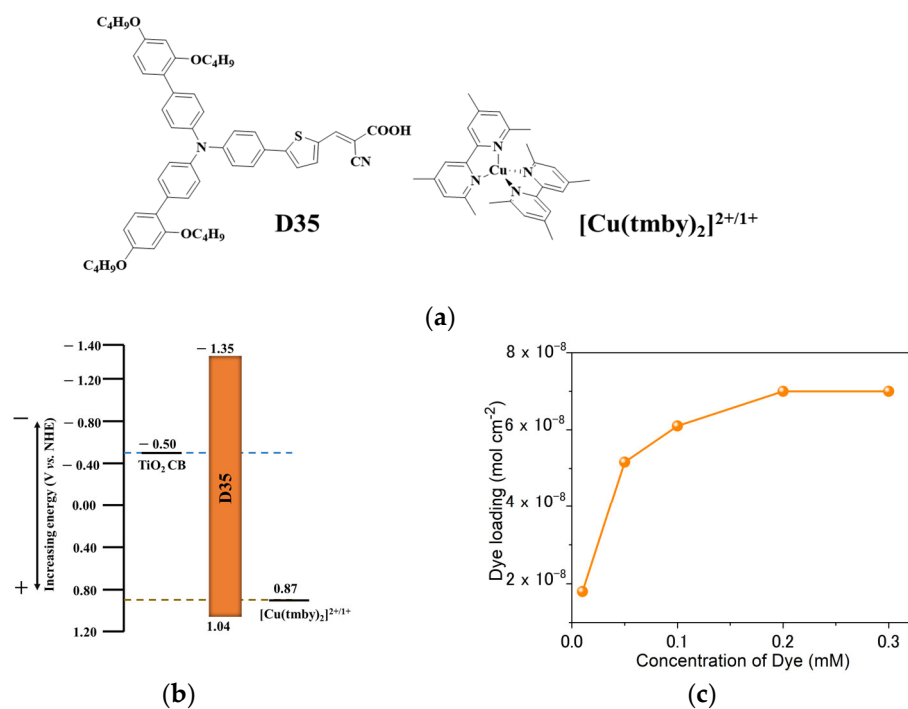


Figure 1. (a,b) Structure and energetics of D35 dye and [Cu(tmby)₂]^{2+/1+} redox mediator and (c) dye loading as a function of dye concentration on TiO₂ films.

Current density–voltage (J–V) characteristics were carried out under one-sun (AM 1.5 G, 100 mW/cm²) illumination (Figure 2a) and the resultant photovoltaic parameters are summarized in Table 1. The J_{sc} obtained from J–V measurements followed a similar trend to the IPCE response (Figure 2b). We observed improvement in V_{oc}, J_{sc}, FF, and hence PCE with an increase in dye concentration. The optimum PCE of 6.50 ± 0.25% (V_{oc}-1002 ± 3 mV, J_{sc}-10.22 ± 0.25 mA/cm², and FF-0.63 ± 0.01) was obtained for DSCs fabricated using 0.1 mM dye concentration. Further, the increase in dye concentration contributed towards the drop in V_{oc}, J_{sc}, and PCE, while FF remained unaltered. A similar trend was also observed for DSCs measured at various light intensities ranging from 0.1 sun to 1 sun. Figure 3 shows photovoltaic parameters of DSCs at various dye concentrations from 0.1 sun to 1 sun; the corresponding values are given in Table S1.

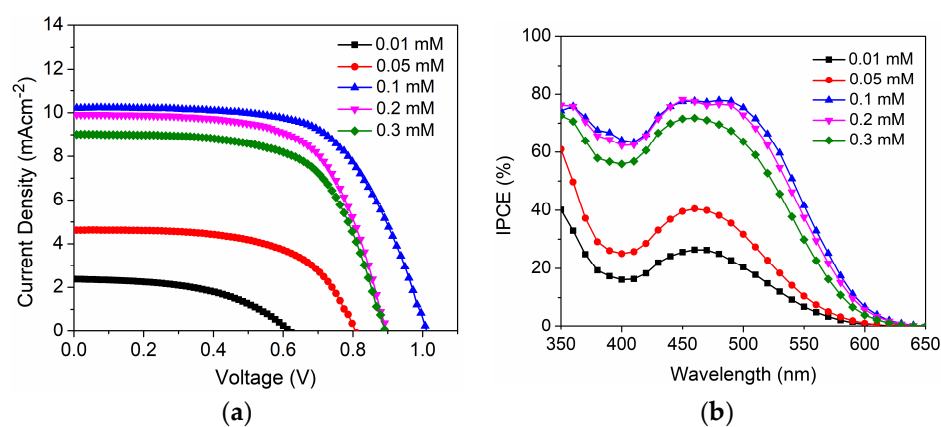
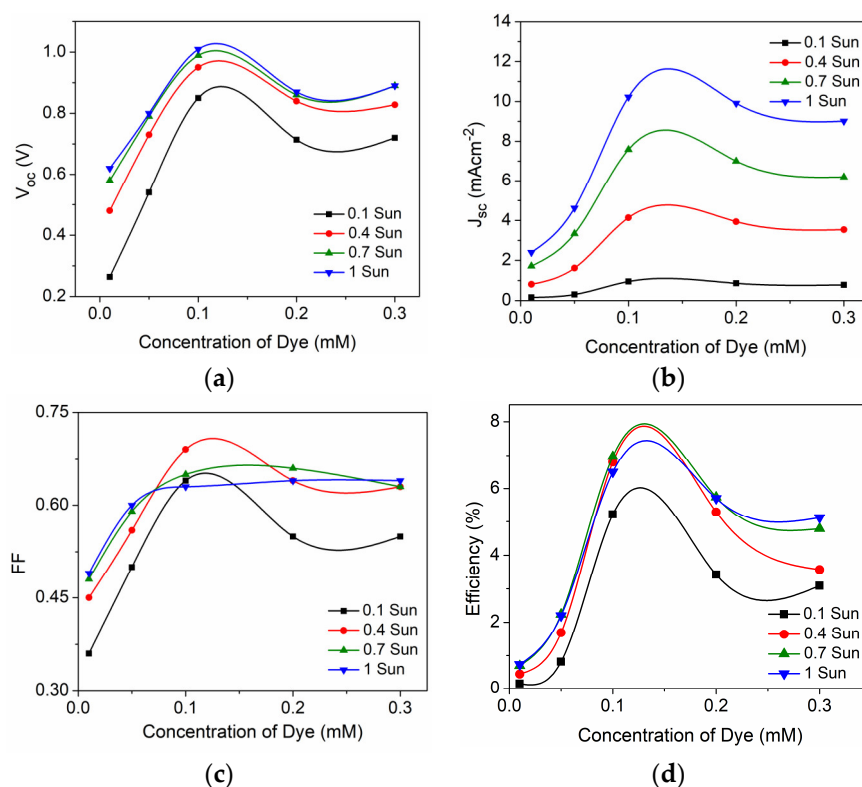


Figure 2. (a) Current density–voltage (J–V) and (b) incident photon current conversion efficiency (IPCE) plot of DSCs fabricated with various D35 dye concentrations along with [Cu(tmby)₂]^{2+/1+} redox mediator under one-sun illumination.

Table 1. Photovoltaic parameters of DSCs fabricated with various D35 dye concentrations along with $[\text{Cu}(\text{tmby})_2]^{2+/1+}$ redox mediator under one-sun illumination.

D35 Concentration (mM)	V_{oc} (mV)	J_{sc} (mAcm^{-2})	FF	η (%)
0.01	622 ± 2	2.40 ± 0.48	0.49 ± 0.02	0.73 ± 0.12
0.05	803 ± 3	4.62 ± 0.37	0.60 ± 0.01	2.22 ± 0.18
0.1	1002 ± 3	10.22 ± 0.25	0.63 ± 0.01	6.50 ± 0.25
0.2	898 ± 4	9.91 ± 0.28	0.64 ± 0.03	5.70 ± 0.26
0.3	895 ± 6	9.09 ± 0.27	0.64 ± 0.02	5.12 ± 0.21

**Figure 3.** Photovoltaic parameter of DSCs with D35 sensitizer and $[\text{Cu}(\text{tmby})_2]^{2+/1+}$ electrolyte (a) V_{oc} , (b) J_{sc} , (c) FF and (d) efficiency from 0.1 sun to 1 sun as a function of dye concentration (0.01 mM, 0.05 mM, 0.1 mM, 0.2 mM, and 0.3 mM).

Indoor photovoltaic characterization was carried out using a homemade indoor light simulator using warm white CFL light source. Figure 4 shows the current density–voltage (J–V) and power curves (P–V) for DSCs fabricated using various dye concentrations under 1000 lux CFL illumination. The indoor photovoltaic parameters are summarized in Table 2. The photovoltaic performance under 1000 lux illumination followed the same trend of 1 sun, but with enhanced efficiencies. Higher efficiency under CFL illumination is attributed to the better spectral overlap of the emission spectrum of CFL with the absorption of the D35 sensitizer. The highest PCE of $10.48 \pm 0.30\%$ (V_{oc} -773 \pm 3 mV, J_{sc} -48.8 \pm 0.9 μAcm^{-2} , and FF-0.78 \pm 0.02) was achieved at 0.1 mM dye concentration. Notably, under 1000 lux illumination, a superior fill factor was observed compared to 1 sun conditions. This is due to reduced recombination at 1000 lux, which is attributed to a lower photoinduced charge density. A similar trend in photovoltaic performance was also observed for DSCs measured at various light intensities ranging from 200 lux to 1000 lux (Figure S1, Table S2).

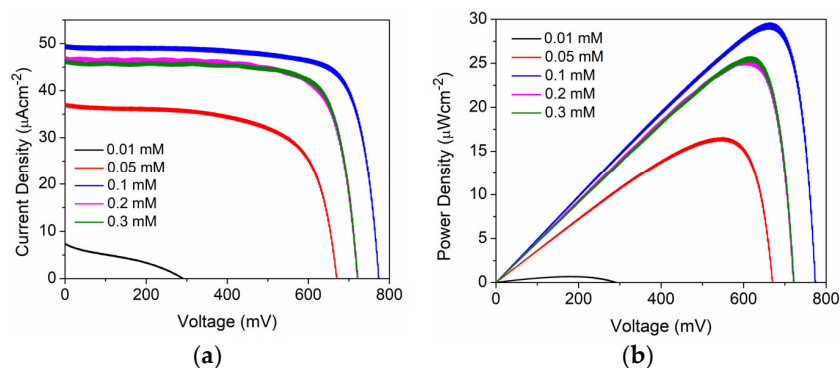


Figure 4. (a) Current density–voltage (J-V) and (b) power curve for DSCs fabricated with different D35 dye concentrations along with $[\text{Cu}(\text{tmby})_2]^{2+/1+}$ redox mediator under 1000 lux illumination.

Table 2. Photovoltaic parameters of DSCs fabricated with various D35 dye concentrations along with $[\text{Cu}(\text{tmby})_2]^{2+/1+}$ redox mediator under 1000 lux CFL illumination.

D35 Concentration (mM)	V_{oc} (mV)	J_{sc} (μAcm^{-2})	FF	η (%)
0.01	292 ± 6	7.4 ± 0.8	0.32 ± 0.02	2.4 ± 0.22
0.05	670 ± 2	37 ± 0.9	0.66 ± 0.03	5.84 ± 0.13
0.1	773 ± 3	48.8 ± 0.9	0.78 ± 0.02	10.48 ± 0.30
0.2	721 ± 2	46.8 ± 0.6	0.76 ± 0.01	9.17 ± 0.12
0.3	721 ± 2	46.4 ± 0.2	0.77 ± 0.08	9.09 ± 0.21

3.2. Interfacial Charge Transfer Study

Interfacial charge transfer analysis of the fabricated dye-sensitized solar cells provides a better understanding of the fundamental processes happening at various interfaces that dictate the PV performance. In the present study, we relied on various electro-optical perturbations and pump-probe techniques in addition to steady state current-voltage (I-V) measurements to understand the fundamental charge transfer process occurring in different interface of DSCs as a function of the amount of dye on semiconductor. As copper redox mediators are often limited by mass transport, we analyzed J_{sc} vs. light intensity measurement to probe the mass transport (Figure 5). Generally, J_{sc} increases with an increase in input light illumination by the relation, $J_{sc} \propto I^\alpha$, where α is the power constant. α was found to be nearly one for DSCs with different dye loading amounts, suggesting a minimal influence of dye loading on the mass transport [43]. We observed similar results in our previous study, where DSCs consisting of D35 dye and $[\text{Cu}(\text{tmby})_2]^{2+/1+}$ were found to be free from mass transport [44]. This could be attributed to the smaller size of the D35 sensitizer, which provides ample space for the electrolyte to penetrate in a working device.

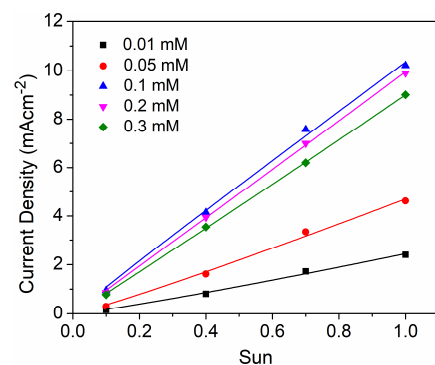


Figure 5. Current density as a function of light intensity for DSCs fabricated with various D35 dye concentrations using $[\text{Cu}(\text{tmby})_2]^{2+/1+}$.

The difference between the Fermi energy level of TiO₂ and the redox potential of electrolyte accounts for V_{oc} and is related to light intensity (I) by the equation [45,46].

$$(dV_{oc})/d\log I = (2.30 m k_B T)/q \quad (1)$$

where m is the ideality factor, k_B is the Boltzmann constant, T is the temperature, and q is the charge. Figure 6a represents V_{oc} as a function of irradiance under outdoor light conditions, Figure 6b displays V_{oc} as a function of illuminance under indoor light conditions, and Figure 6c shows the ideality factor at various dye concentrations. Generally, the relation between V_{oc} and I is non-ideal in DSCs, which originates from interfacial charge recombination from trap states [47]. Here, we observed a non-ideal relation between V_{oc} and I with an m value ranging from 2.7 to 5.8 under outdoor illumination and 3.9 to 14.4 under indoor illumination. As observed from Figure 6c, under both outdoor and indoor illumination, the m value decreased with increase in dye concentration and reached a minimum value of 0.1 mM dye concentration, while it further increased at higher concentrations of dye. It is to be noted that the deviation from ideal behavior is more pronounced under indoor light illumination, indicating the need to control recombination to realize higher photovoltaic performance under indoor/artificial illuminations. According to Bisquert et al., the non-ideal characteristics observed are related to the electron recombination not only from the conduction band of TiO₂, but also from the surface states and trap states distributed exponentially in the band gap of TiO₂ [48,49]. Further, Zhang et al. also observed a deviation in the ideality factor for DSCs using different organic sensitizers; for instance, DSCs with NT5 sensitizer showed an m value of 1.7 while MS4 and MS5 showed an m value of 1.26 and 1.04, respectively [8]. The difference in the ideality factor was mainly attributed to the reduction in interfacial charge recombination from the surface and trap states. Thus, in the present context, it can be said that an optimum concentration of dye molecules on TiO₂ is necessary to passivate the surface states for lower recombination. To clarify this further, we measured the dark current of DSCs (Figure 6d) with various dye loading amounts. Herein we also included a device without any dye to quantify the role of dyes in preventing interfacial charge recombination. As seen in Figure 6d with the increase in dye concentration dark current reduced rapidly and reached a minimum value at 0.1 mM dye concentration while it again increased at higher dye concentrations. The trend in dark current aligns with the calculated ideality factor (Figure 6c), which confirms that the dye molecules are capable of regulating recombination at TiO₂/electrolyte interface and a careful optimization of dye concentration is inevitable to extract the best performance from these devices particularly employing organic with alternate Cu(II/I) redox mediators.

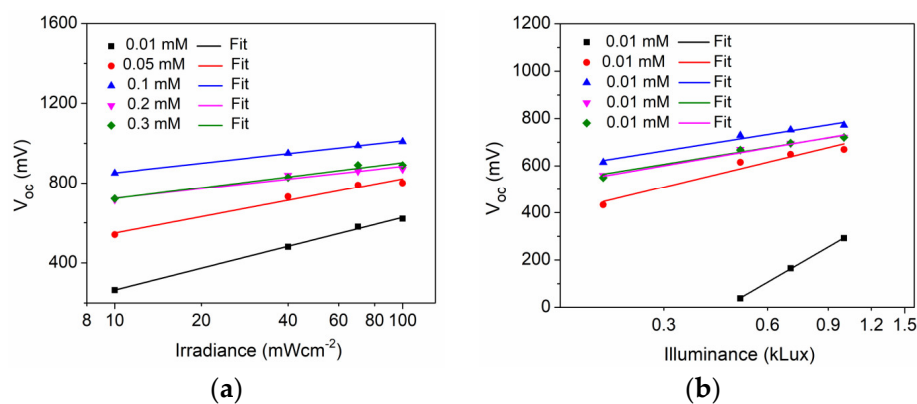


Figure 6. Cont.

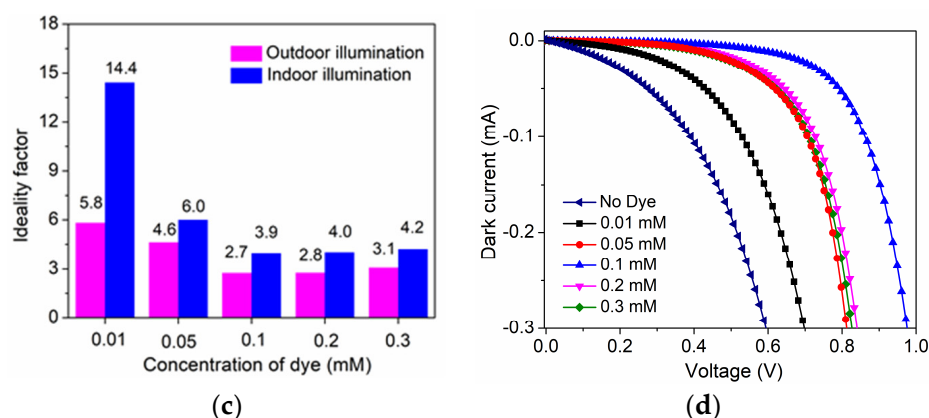


Figure 6. V_{oc} as a function of (a) irradiance (mW/cm^2) under 1 sun irradiation ($100 \text{ mW}/\text{cm}^2$), (b) illuminance (lux) under indoor light illuminations, (c) ideality factor calculated as a function of D35 dye concentration under solar and indoor CFL illumination and (d) dark current as a function of D35 dye concentration.

For a detailed interfacial charge transfer study, we used electrochemical impedance spectroscopic (EIS) measurements under dark conditions. In TiO_2 photoanode, diffusion and recombination of injected electrons, occur simultaneously. As dye molecules are placed between TiO_2 and electrolyte, it undoubtedly influences the charge dynamics at the TiO_2 /electrolyte interface. EIS is considered to be the most reliable characterization tool to probe charge transfer processes, as both transport time and lifetime can simultaneously be extracted at the same Fermi level position. On the contrary, employing other perturbation tools, the lifetime is measured at open circuit condition and transport time is measured at short circuit condition. EIS measurements were carried out at different steady-state voltages with a constant perturbation amplitude of 10 mV at frequencies starting from 100 mHz to 100 kHz. The representative Nyquist plot and Bode plot at 0.85 V for different D35 dye concentrations are given in Figure 7a,b. The impedance plots were fitted using an equivalent circuit with a transmission line model given in Figure 7c [50,51]. The Nyquist plot consists of three semicircles, where the first semicircle at a higher frequency corresponds to the charge transfer at the counter/electrolyte interface, the second semicircle at the intermediate frequency corresponds to charge transfer at TiO_2 /dye/electrolyte interface, and the semicircle at the lower frequency region represents the diffusion of ions in the bulk electrolyte. The equivalent circuit consists of resistors, capacitors and constant phase element. R_{PEDOT} and C_{PEDOT} refer to resistance and capacitance at the counter electrode/electrolyte interface. Similarly, R_s corresponds to the sheet resistance of the substrates, Z_d represents the impedance of ion diffusion in electrolyte, R_t corresponds to the resistance of electrons to diffuse in mesoporous TiO_2 , R_{rec} is the charge transfer resistance at the TiO_2 /dye/electrolyte interface, and C_μ is the constant phase element representing the capacitance at the TiO_2 /electrolyte interface. As observed in Figure 7a, the size of the first semicircle and third semicircle remained unaltered with change in dye concentration, which suggests that charge transfer at the counter electrode/electrolyte interface and ion diffusion in the electrolyte, bulk are not influenced by the change in dye concentrations. A significant change in the middle semicircle suggests that the charge transfer at the TiO_2 /dye/electrolyte interface is primarily influenced by variation in dye concentrations. A similar feature was also observed in the Bode plot, where peaks at low and high frequency did not change, while a significant change in peaks at intermediate frequencies was observed.

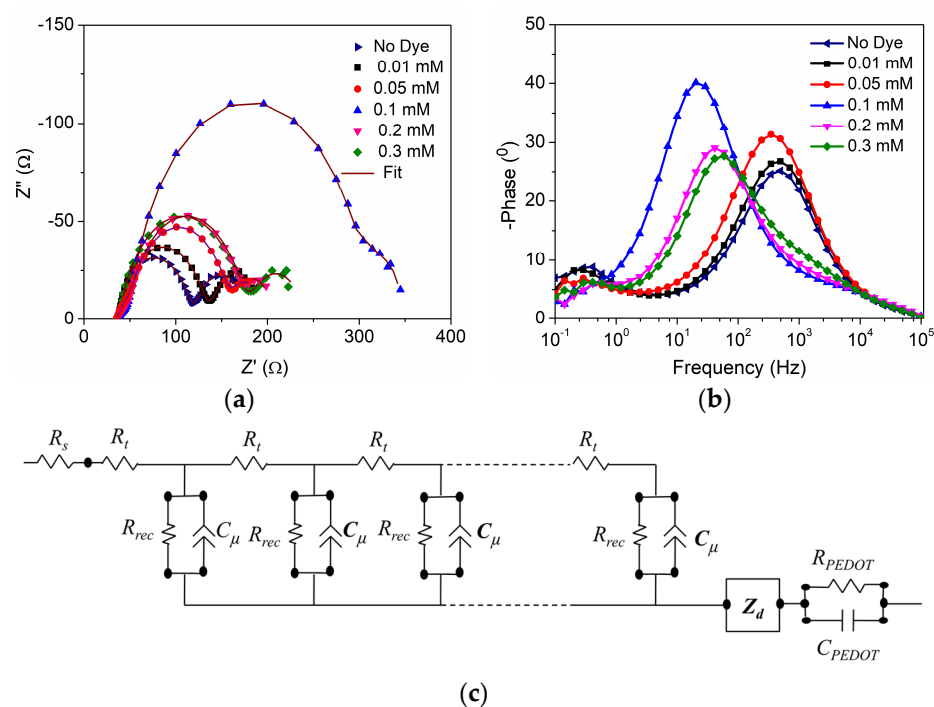


Figure 7. (a) Nyquist plot, (b) Bode plot, and (c) equivalent circuit used for fitting the obtained Nyquist plot for DSCs with different D35 concentrations employing $[\text{Cu}(\text{tmb})_2]^{2+/1+}$ electrolyte.

The accumulation of electrons at the $\text{TiO}_2/\text{electrolyte}$ interface is quantified using capacitance. Here constant phase element is used in place of capacitance to obtain a better fitting. Figure 8a shows C_μ as a function of Fermi voltage (V_F). V_F is calculated from the equation:

$$V_F = V_{\text{applied}} - IR_{\text{eqv}} \quad (2)$$

where, V_{applied} is the steady state voltage applied across the device during EIS measurement, I is the obtained current, and R_{eqv} is the total series resistance (i.e., summation of sheet resistance (R_s), counter electrode resistance (R_{pedot}) and diffusion resistance (R_d). C_μ is generally used to locate the conduction band (CB) of TiO_2 . The CB of TiO_2 for DSCs with 0 mM, 0.01 mM, and 0.05 mM dye concentration lies at similar energy levels. Likewise, the CB of TiO_2 for DSCs with higher dye concentrations of 0.1 mM, 0.2 mM, and 0.3 mM also remains at similar energy levels. However, they are shifted to more positive potentials compared to the device at lower concentrations. Generally, dye molecules bind to the TiO_2 by releasing protons, which contributes in shifting the conduction band of TiO_2 to a more positive potential [52]. Thus, at higher dye concentrations (0.1 mM, 0.2 mM, 0.3 mM), the number of released protons were sufficient enough to shift the CB of TiO_2 positive potentials. Very often, a positive shift in CB of TiO_2 helps to improve J_{sc} by providing a better driving force for electron injection from LUMO of the sensitizer to TiO_2 . Since we used a D35 sensitizer with high negative excited state potentials (-1.35 V, Figure 1b), a minimal influence in J_{sc} owing to a CB shift is expected. It is further explored using photoinduced absorption (PIA) spectroscopy in upcoming discussions. Moreover, the improvement in J_{sc} is largely associated with better dye loading at higher dye concentrations.

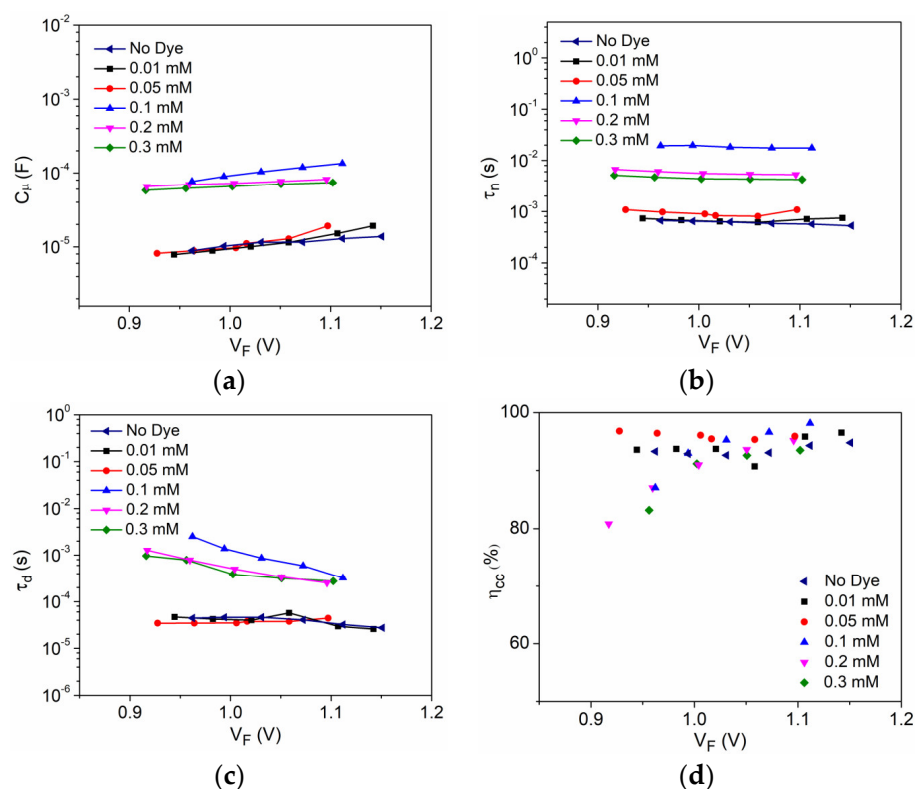


Figure 8. (a) Chemical capacitance (C_{μ}), (b) lifetime (τ_n), (c) transport time (τ_d), and (d) charge collection efficiency (η_{cc}) as a function of V_F for DSCs with different dye concentrations using D35 sensitizer and $[\text{Cu}(\text{tmby})_2]^{2+/1+}$ electrolyte.

As seen in Figure 8b, there is a lifetime upsurge with the increase in dye concentration that reaches a maximum at 0.1 mM D35 dye concentration. Subsequent increases in dye concentration led to a decline in lifetime. The same trend was also observed from Nyquist and Bode plots (Figure 7). A similar trend in recombination was also previously observed by Boschloo and co-workers in DSCs fabricated using D35 dye and $[\text{Co}(\text{bpy})_3]^{3+/2+}$ redox mediator [37]. The increasing trend in lifetime with increased dye loading is mainly attributed to better coverage of dye molecules over the TiO_2 surface. However, at higher dye concentrations (0.1 mM, 0.2 mM and 0.3 mM) there is a positive shift in CB of TiO_2 as evident from the capacitance plot (Figure 8a), which also reduces the recombination driving force. Recombination from the bandgap and sub bandgap states are more prominent in copper electrolyte DSCs. Thus, reducing the recombination driving force along with better passivation of TiO_2 by dyes helped in controlling the photovoltaic performance. Optimum performance was delivered by DSCs using 0.1 mM dye concentration. Further, with an increase in concentration (>0.1 mM), we observed a reduction in lifetime. But we did not observe any change in CB of TiO_2 at higher concentrations (Figure 8a), which indicates that the observed decrease in lifetime is associated with more recombination at higher concentrations. The trend in lifetime was also reflected and related to the observed open circuit potential (V_{oc}) (Table 1). DSCs fabricated with 0.1 mM D35 dye solution provided uniform surface coverage of TiO_2 that spatially separates the oxidized Cu(II) species moving closer to TiO_2 . Additionally, devices fabricated using 0.1 mM D35 dye resulted in the lowest recombination driving force. Both the above factors contributed to higher photovoltaic performance using 0.1 mM D35 concentration. Lifetime also followed the same trend as that of the ideality factor and dark current (Figure 6c,d). The transport time (τ_d) measured from EIS (Figure 8c) shows faster transport for devices with lower dye concentrations. The charge collection efficiency obtained from EIS showed better collection employing 0.1 mM D35.

We further used photoinduced absorption spectroscopy (PIA) to analyze the electron injection and dye regeneration of DSCs fabricated with different D35 concentrations. Figure 9a,b shows PIA as a function of wavelength, for dye soaked photoanodes in the absence and presence of the $[\text{Cu}(\text{tmby})_2]^{2+/1+}$ redox mediator, respectively. The absorption of oxidized D35 dye under different dye concentrations was observed after the 700 nm wavelength region (Figure 9a). Further, in the presence of a redox mediator, the absorption response is quenched, which reflects efficient dye regeneration. As the PIA spectra for all the dye concentrations overlap with and without electrolytes, a similar rate of electron injection and dye regeneration is expected for DSCs with various dye concentrations. In short, it can be said that variation of dye coverage over the TiO_2 surface has little influence on injection and regeneration and does not likely modify the structural and energetic behavior of DSCs to influence the J_{sc} employing the D35 sensitizer and $[\text{Cu}(\text{tmby})_2]^{2+/1+}$ electrolyte. Thus, the observed variations in short-circuit current density (J_{sc}) unequivocally depend on the discrepancies in dye loading and the resultant disparities in light harvesting properties of the sensitizer. Similarly, the variations in voltage are intricately linked to variations in the recombination dynamics and lifetime of the devices.

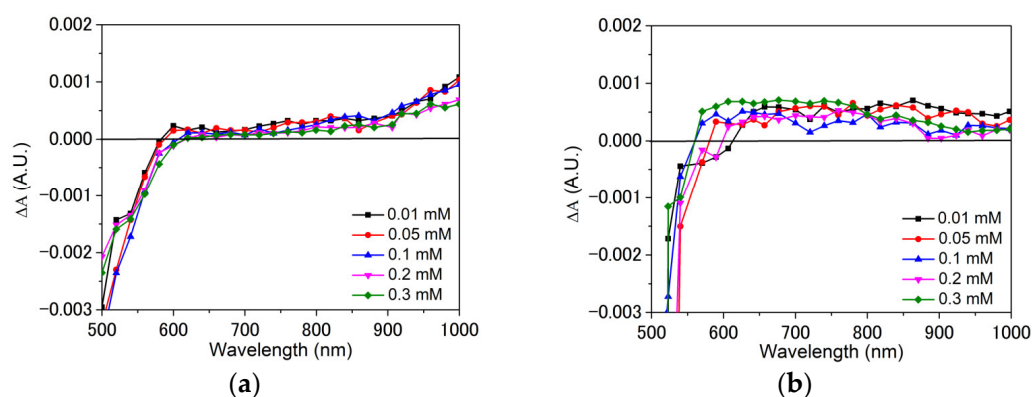


Figure 9. (a) Injection and (b) regeneration plot measured using photo-induced absorption (PIA) spectroscopy for devices fabricated using D35 sensitizer and $[\text{Cu}(\text{tmby})_2]^{2+/1+}$ electrolyte under various dye concentrations.

4. Discussion

We studied the role of dye molecules in regulating the charge transfer dynamics of DSCs employing alternate copper redox mediators. In the present study, D35 organic dye at various dye concentrations (0.01 mM, 0.05 mM, 0.1 mM, 0.2 mM, and 0.3 mM) was used along with a $[\text{Cu}(\text{tmby})_2]^{2+/1+}$ redox mediator. With the increase in dye concentration, dye loading over the TiO_2 surface was found to increase and reached saturation at 0.2 mM D35 concentration. However, 0.1 mM dye concentration was found to be optimal in terms of photovoltaic performance. A maximum power conversion of $6.50 \pm 0.25\%$ under the full sun ($100 \text{ mW}/\text{cm}^2$) and $10.48 \pm 0.30\%$ under indoor illumination (1000 lux CFL) was obtained for devices fabricated using 0.1 mM D35 concentration. The calculated ideality factor (m) was also more reasonable at 0.1 mM D35 concentration under full sun and indoor light illuminations. It is important to note that DSCs showed more deviation from ideal behavior under indoor illumination than under full sun, indicating the importance of addressing recombination at lower illumination intensities. Further, the ideality factor was also in line with the obtained dark current results. EIS was carried out under dark conditions for devices fabricated without the dye and with varying dye concentrations to gain better knowledge on interfacial charge transfer dynamics dye coverage over TiO_2 . The conduction band of TiO_2 was found to shift towards positive potentials with increase in dye concentrations (0.1 mM, 0.2 mM, and 0.3 mM). Likewise, lifetime was also found to increase with dye concentration, and the best lifetime was showcased by devices fabricated using 0.1 mM dye, which further dropped at higher dye concentrations (0.2 mM and

0.3 mM). The increase in lifetime is mainly attributed to the better dye coverage and reduced recombination driving force associated with the positive shift in CB. In contrast, the drop in lifetime at higher dye concentrations may be due to disordered dye distribution over TiO₂. Moreover, 0.1 mM dye concentration also delivered the best charge collection efficiency among the series. The electron injection and regeneration were found to be quite similar under various concentrations. The targeted applications under indoor photovoltaic domain demands for higher V_{oc} and a better control on V_{oc} achieved by changing dye concentration provides better insights, to further improve the V_{oc} in organic dye-copper electrolyte DSCs. With the optimal surface coverage achieved using 0.1 mM D35 dye concentration, DSCs delivered a V_{oc} of 1000 mV under 1 sun and 773 mV under 1000 lux illumination. In a nutshell, variation of dye content over TiO₂ surface not only modifies J_{sc} but also changes V_{oc} and FF of DSC. Thus, an optimum dye concentration is essential to realize better photovoltaic performance by employing organic dye-copper electrolyte combination under outdoor and indoor illumination.

Supplementary Materials: The following supporting information can be downloaded at: <https://www.mdpi.com/article/10.3390/en16196913/s1>. Table S1. Photovoltaic parameters of DSCs with D35 sensitizer and [Cu(tmby)₂]^{2+/1+} electrolyte under various outdoor illuminations. Table S2. Photovoltaic parameters of DSCs with D35 sensitizer and [Cu(tmby)₂]^{2+/1+} electrolyte under various indoor illuminations. Figure S1. Photovoltaic characteristics of DSCs with D35 sensitizer and [Cu(tmby)₂]^{2+/1+} electrolyte (a) V_{oc}, (b) J_{sc}, (c) FF and (d) efficiency from 0.1 sun to 1 sun as a function of dye concentration (0.01 mM, 0.05 mM, 0.1 mM, 0.2 mM, and 0.3 mM) under indoor illumination.

Author Contributions: Conceptualization, S.C.P.; methodology, S.C.P.; software, S.C.P. and J.V.; validation, S.C.P., J.V. and S.M.M.; formal analysis, S.C.P. and J.V.; investigation, S.C.P. and J.V.; resources, S.S.; data curation, S.C.P. and J.V.; writing—original draft preparation, S.C.P.; writing—review and editing, S.C.P.; supervision, S.S.; project administration, S.S.; funding acquisition, S.S. All authors have read and agreed to the published version of the manuscript.

Funding: We acknowledge financial support from SERB CRG project (CRG/2020/001406), CSIR-FIRST project (MLP65), DST Solar Challenge Award (DST/ETC/CASE/RE5/2023/05(C)&(G)), CSIR-FTT project (MLP74), DST-Nanomission (GAP 1629) and DST-ICMAP project (DST/TMD/ICMAP/2K20/03). S.C.P. acknowledges CSIR for the research fellowship.

Data Availability Statement: Not applicable.

Conflicts of Interest: The authors declare no conflict of interest.

References

1. Sohani, A.; Memon, S.; Hoseinzadeh, S.; Garcia, D.A.; Schoden, F.; Detzmeier, J.; Schnatmann, A.K.; Blachowicz, T.; Schwenzfeier-Hellkamp, E. Investigating the Remanufacturing Potential of Dye-Sensitized Solar Cells. *Sustainability* **2022**, *14*, 5670. [CrossRef]
2. Syed, T.H.; Wei, W. Technoeconomic Analysis of Dye Sensitized Solar Cells (DSSCs) with WS₂/Carbon Composite as Counter Electrode Material. *Inorganics* **2022**, *10*, 191. [CrossRef]
3. Enaganti, P.K.; Soman, S.; Devan, S.S.; Pradhan, S.C.; Srivastava, A.K.; Pearce, J.M.; Goel, S. Dye-sensitized Solar Cells as Promising Candidates for Underwater Photovoltaic Applications. *Prog. Photovolt. Res. Appl.* **2022**, *30*, 632–639. [CrossRef]
4. Aslam, A.; Mehmood, U.; Arshad, M.H.; Ishfaq, A.; Zaheer, J.; Ul Haq Khan, A.; Sufyan, M. Dye-Sensitized Solar Cells (DSSCs) as a Potential Photovoltaic Technology for the Self-Powered Internet of Things (IoTs) Applications. *Sol. Energy* **2020**, *207*, 874–892. [CrossRef]
5. Mariotti, N.; Bonomo, M.; Fagiolari, L.; Barbero, N.; Gerbaldi, C.; Bella, F.; Barolo, C. Recent Advances in Eco-Friendly and Cost-Effective Materials towards Sustainable Dye-Sensitized Solar Cells. *Green Chem.* **2020**, *22*, 7168–7218. [CrossRef]
6. Sadow, E.; Raut, P.; Kishnani, V.; Mondal, K.; Gupta, A.; Jana, S.C. A Review on Gel Polymer Electrolytes for Dye-Sensitized Solar Cells. *Micromachines* **2022**, *13*, 680. [CrossRef]
7. Kokkonen, M.; Talebi, P.; Zhou, J.; Asgari, S.; Soomro, S.A.; Elsehrawy, F.; Halme, J.; Ahmad, S.; Hagfeldt, A.; Hashmi, S.G. Advanced Research Trends in Dye-Sensitized Solar Cells. *J. Mater. Chem. A* **2021**, *9*, 10527–10545. [CrossRef]
8. Zhang, D.; Stojanovic, M.; Ren, Y.; Cao, Y.; Eickemeyer, F.T.; Socie, E.; Vlachopoulos, N.; Moser, J.E.; Zakeeruddin, S.M.; Hagfeldt, A.; et al. A Molecular Photosensitizer Achieves a V_{oc} of 1.24 V Enabling Highly Efficient and Stable Dye-Sensitized Solar Cells with Copper(II/I)-Based Electrolyte. *Nat. Commun.* **2021**, *12*, 1777. [CrossRef]

9. Michaels, H.; Rinderle, M.; Freitag, R.; Benesperi, I.; Edvinsson, T.; Socher, R.; Gagliardi, A.; Freitag, M. Dye-Sensitized Solar Cells under Ambient Light Powering Machine Learning: Towards Autonomous Smart Sensors for the Internet of Things. *Chem. Sci.* **2020**, *11*, 2895–2906. [[CrossRef](#)]
10. Haridas, R.; Velore, J.; Pradhan, S.C.; Vindhyasarumi, A.; Yoosaf, K.; Soman, S.; Unni, K.N.N.; Ajayaghosh, A. Indoor Light-Harvesting Dye-Sensitized Solar Cells Surpassing 30% Efficiency without Co-Sensitizers. *Mater. Adv.* **2021**, *2*, 7773–7787. [[CrossRef](#)]
11. Roy, A.; Ghosh, A.; Bhandari, S.; Selvaraj, P.; Sundaram, S.; Mallick, T.K. Color Comfort Evaluation of Dye-Sensitized Solar Cell (DSSC) Based Building-Integrated Photovoltaic (BIPV) Glazing after 2 Years of Ambient Exposure. *J. Phys. Chem. C* **2019**, *123*, 23834–23837. [[CrossRef](#)]
12. Lee, H.M.; Yoon, J.H. Power Performance Analysis of a Transparent DSSC BIPV Window Based on 2 Year Measurement Data in a Full-Scale Mock-Up. *Appl. Energy* **2018**, *225*, 1013–1021. [[CrossRef](#)]
13. Park, B.R.; Choi, E.J.; Choi, Y.J.; Moon, J.W. Environmental and Energy Performance Analysis of DSSC BIPV Window in Office Buildings. *KIEAE J.* **2020**, *20*, 121–128. [[CrossRef](#)]
14. Kim, H.; Jo, J.; Lee, G.; Shin, M.; Lee, J.-C. Design and Analysis of a Highly Reliable Large-Area Z-Type Transparent Module for Dye-Sensitized Solar Cells. *Sol. Energy* **2017**, *155*, 585–592. [[CrossRef](#)]
15. Barichello, J.; Vesce, L.; Mariani, P.; Leonardi, E.; Braglia, R.; Di Carlo, A.; Canini, A.; Reale, A. Stable Semi-Transparent Dye-Sensitized Solar Modules and Panels for Greenhouse Application. *Energies* **2021**, *14*, 6393. [[CrossRef](#)]
16. Muñoz-García, A.B.; Benesperi, I.; Boschloo, G.; Concepcion, J.J.; Delcamp, J.H.; Gibson, E.A.; Meyer, G.J.; Pavone, M.; Pettersson, H.; Hagfeldt, A.; et al. Dye-Sensitized Solar Cells Strike Back. *Chem. Soc. Rev.* **2021**, *50*, 12450–12550. [[CrossRef](#)]
17. Jiang, R.; Michaels, H.; Vlachopoulos, N.; Freitag, M. Beyond the Limitations of Dye-Sensitized Solar Cells. In *Dye-Sensitized Solar Cells*; Elsevier: Amsterdam, The Netherlands, 2019; pp. 285–323. [[CrossRef](#)]
18. Yella, A.; Humphry-Baker, R.; Curchod, B.F.E.; Ashari Astani, N.; Teuscher, J.; Polander, L.E.; Mathew, S.; Moser, J.-E.; Tavernelli, I.; Rothlisberger, U.; et al. Molecular Engineering of a Fluorene Donor for Dye-Sensitized Solar Cells. *Chem. Mater.* **2013**, *25*, 2733–2739. [[CrossRef](#)]
19. Sivasankaran, L.; Pradhan, S.C.; Mishra, R.K.; Soman, S.; Ajayaghosh, A. Role of Alkyl Groups Regulating Recombination and Mass Transport at Cobalt Electrolyte-Dye Interface in Dye Sensitized Solar Cells. *Sol. Energy* **2022**, *236*, 182–194. [[CrossRef](#)]
20. Zhang, W.; Wu, Y.; Bahng, H.W.; Cao, Y.; Yi, C.; Saygili, Y.; Luo, J.; Liu, Y.; Kavan, L.; Moser, J.-E.; et al. Comprehensive Control of Voltage Loss Enables 11.7% Efficient Solid-State Dye-Sensitized Solar Cells. *Energy Environ. Sci.* **2018**, *11*, 1779–1787. [[CrossRef](#)]
21. Gangadhar, P.S.; Jagadeesh, A.; Rajesh, M.N.; George, A.S.; Prasanthkumar, S.; Soman, S.; Giribabu, L. Role of π -Spacer in Regulating the Photovoltaic Performance of Copper Electrolyte Dye-Sensitized Solar Cells Using Triphenylimidazole Dyes. *Mater. Adv.* **2022**, *3*, 1231–1239. [[CrossRef](#)]
22. Naim, W.; Novelli, V.; Nikolinakos, I.; Barbero, N.; Dzeba, I.; Grifoni, F.; Ren, Y.; Alnasser, T.; Velardo, A.; Borrelli, R.; et al. Transparent and Colorless Dye-Sensitized Solar Cells Exceeding 75% Average Visible Transmittance. *JACS Au* **2021**, *1*, 409–426. [[CrossRef](#)]
23. Hualmé, Q.; Mwalukuku, V.M.; Joly, D.; Liotier, J.; Kervella, Y.; Maldivi, P.; Narbey, S.; Oswald, F.; Riquelme, A.J.; Anta, J.A.; et al. Photochromic Dye-Sensitized Solar Cells with Light-Driven Adjustable Optical Transmission and Power Conversion Efficiency. *Nat. Energy* **2020**, *5*, 468–477. [[CrossRef](#)] [[PubMed](#)]
24. Ren, Y.; Zhang, D.; Suo, J.; Cao, Y.; Eickemeyer, F.T.; Vlachopoulos, N.; Zakeeruddin, S.M.; Hagfeldt, A.; Grätzel, M. Hydroxamic Acid Pre-Adsorption Raises the Efficiency of Cosensitized Solar Cells. *Nature* **2022**, *613*, 60–65. [[CrossRef](#)]
25. Michaels, H.; Benesperi, I.; Freitag, M. Challenges and Prospects of Ambient Hybrid Solar Cell Applications. *Chem. Sci.* **2021**, *12*, 5002–5015. [[CrossRef](#)]
26. Freitag, M.; Boschloo, G. The Revival of Dye-Sensitized Solar Cells. *Curr. Opin. Electrochem.* **2017**, *2*, 111–119. [[CrossRef](#)]
27. Freitag, M.; Teuscher, J.; Saygili, Y.; Zhang, X.; Giordano, F.; Liska, P.; Hua, J.; Zakeeruddin, S.M.; Moser, J.E.; Grätzel, M.; et al. Dye-Sensitized Solar Cells for Efficient Power Generation under Ambient Lighting. *Nat. Photonics* **2017**, *11*, 372–378. [[CrossRef](#)]
28. Saygili, Y.; Söderberg, M.; Pellet, N.; Giordano, F.; Cao, Y.; Muñoz-García, A.B.; Zakeeruddin, S.M.; Vlachopoulos, N.; Pavone, M.; Boschloo, G.; et al. Copper Bipyridyl Redox Mediators for Dye-Sensitized Solar Cells with High Photovoltage. *J. Am. Chem. Soc.* **2016**, *138*, 15087–15096. [[CrossRef](#)]
29. Freitag, M.; Giordano, F.; Yang, W.; Pazoki, M.; Hao, Y.; Zietz, B.; Grätzel, M.; Hagfeldt, A.; Boschloo, G. Copper Phenanthroline as a Fast and High-Performance Redox Mediator for Dye-Sensitized Solar Cells. *J. Phys. Chem. C* **2016**, *120*, 9595–9603. [[CrossRef](#)]
30. Li, J.; Yang, X.; Yu, Z.; Gurzadyan, G.G.; Cheng, M.; Zhang, F.; Cong, J.; Wang, W.; Wang, H.; Li, X.; et al. Efficient Dye-Sensitized Solar Cells with [Copper(6,6'-Dimethyl-2,2'-Bipyridine)₂]^{2+/1+} Redox Shuttle. *RSC Adv.* **2017**, *7*, 4611–4615. [[CrossRef](#)]
31. Jagadeesh, A.; Veerappan, G.; Devi, P.S.; Narayanan Unni, K.N.; Soman, S. Synergetic Effect of TiO₂/ZnO Bilayer Photoanodes Realizing Exceptionally High VOC for Dye-Sensitized Solar Cells under Outdoor and Indoor Illuminations. *J. Mater. Chem. A* **2023**, *11*, 14748. [[CrossRef](#)]
32. Wu, H.; Wang, G.; Lei, B.X. Bulky 3D Structures of Dithienopyrrol Dye with Copper(II/I) Redox Mediator Enabling Efficient Solar Cells with an Open-Circuit Voltage of 1.13 V. *ACS Appl. Energy Mater.* **2022**, *5*, 9962–9969. [[CrossRef](#)]
33. Grobelny, A.; Shen, Z.; Eickemeyer, F.T.; Antariksa, N.F.; Zapotoczny, S.; Zakeeruddin, S.M.; Grätzel, M. Molecularly Tailored Photosensitizer with an Efficiency of 13.2% for Dye-Sensitized Solar Cells. *Adv. Mater.* **2022**, *35*, 2207785. [[CrossRef](#)]

34. Tanaka, E.; Michaels, H.; Freitag, M.; Robertson, N. Synergy of Co-Sensitizers in a Copper Bipyridyl Redox System for Efficient and Cost-Effective Dye-Sensitized Solar Cells in Solar and Ambient Light. *J. Mater. Chem. A* **2020**, *8*, 1279–1287. [[CrossRef](#)]
35. Bai, Y.; Yu, Q.; Cai, N.; Wang, Y.; Zhang, M.; Wang, P. High-Efficiency Organic Dye-Sensitized Mesoscopic Solar Cells with a Copper Redox Shuttle. *Chem. Commun.* **2011**, *47*, 4376–4378. [[CrossRef](#)]
36. Tang, X.; Wang, Y.; Cao, G. Effect of the Adsorbed Concentration of Dye on Charge Recombination in Dye-Sensitized Solar Cells. *J. Electroanal. Chem.* **2013**, *694*, 6–11. [[CrossRef](#)]
37. Pazoki, M.; Lohse, P.W.; Taghavinia, N.; Hagfeldt, A.; Boschloo, G. The Effect of Dye Coverage on the Performance of Dye-Sensitized Solar Cells with a Cobalt-Based Electrolyte. *Phys. Chem. Chem. Phys.* **2014**, *16*, 8503. [[CrossRef](#)] [[PubMed](#)]
38. Pradhan, S.C.; Soman, S. Effect of Thickness on Charge Transfer Properties of Conductive Polymer Based PEDOT Counter Electrodes in DSSC. *Results Surf. Interfaces* **2021**, *5*, 100030–100035. [[CrossRef](#)]
39. Ellis, H.; Vlachopoulos, N.; Häggman, L.; Perruchot, C.; Jouini, M.; Boschloo, G.; Hagfeldt, A. PEDOT Counter Electrodes for Dye-Sensitized Solar Cells Prepared by Aqueous Micellar Electrodeposition. *Electrochim. Acta* **2013**, *107*, 45–51. [[CrossRef](#)]
40. Soman, S.; Pradhan, S.C.; Yoosuf, M.; Vinayak, M.V.; Lingamoorthy, S.; Gopidas, K.R. Probing Recombination Mechanism and Realization of Marcus Normal Region Behavior in DSSCs Employing Cobalt Electrolytes and Triphenylamine Dyes. *J. Phys. Chem. C* **2018**, *122*, 14113–14127. [[CrossRef](#)]
41. Feldt, S.M.; Gibson, E.A.; Gabriellson, E.; Sun, L.; Boschloo, G.; Hagfeldt, A. Design of Organic Dyes and Cobalt Polypyridine Redox Mediators for High-Efficiency Dye-Sensitized Solar Cells. *J. Am. Chem. Soc.* **2010**, *132*, 16714–16724. [[CrossRef](#)] [[PubMed](#)]
42. Dryza, V.; Bieske, E.J. Does the Triphenylamine-Based D35 Dye Sensitizer Form Aggregates on Metal-Oxide Surfaces? *J. Photochem. Photobiol. A Chem.* **2015**, *302*, 35–41. [[CrossRef](#)]
43. Velore, J.; Chandra Pradhan, S.; Hamann, T.W.; Hagfeldt, A.; Unni, K.N.N.; Soman, S. Understanding Mass Transport in Copper Electrolyte-Based Dye-Sensitized Solar Cells. *ACS Appl. Energy Mater.* **2022**, *5*, 2647–2654. [[CrossRef](#)]
44. Pradhan, S.C.; Velore, J.; Hagfeldt, A.; Soman, S. Probing Photovoltaic Performance in Copper Electrolyte Dye-Sensitized Solar Cells of Variable TiO₂ Particle Size Using Comprehensive Interfacial Analysis. *J. Mater. Chem. C* **2022**, *10*, 3929–3936. [[CrossRef](#)]
45. Salvador, P.; Hidalgo, M.G.; Zaban, A.; Bisquert, J. Illumination Intensity Dependence of the Photovoltage in Nanostructured TiO₂ Dye-Sensitized Solar Cells. *J. Phys. Chem. B* **2005**, *109*, 15915–15926. [[CrossRef](#)] [[PubMed](#)]
46. Bisquert, J.; Mora-Seró, I. Simulation of Steady-State Characteristics of Dye-Sensitized Solar Cells and the Interpretation of the Diffusion Length. *J. Phys. Chem. Lett.* **2010**, *1*, 450–456. [[CrossRef](#)]
47. Pradhan, S.C.; Hagfeldt, A.; Soman, S. Resurgence of DSCs with Copper Electrolyte: A Detailed Investigation of Interfacial Charge Dynamics with Cobalt and Iodine Based Electrolytes. *J. Mater. Chem. A* **2018**, *6*, 22204–22214. [[CrossRef](#)]
48. Bisquert, J.; Zaban, A.; Greenshtein, M.; Mora-Seró, I. Determination of Rate Constants for Charge Transfer and the Distribution of Semiconductor and Electrolyte Electronic Energy Levels in Dye-Sensitized Solar Cells by Open-Circuit Photovoltage Decay Method. *J. Am. Chem. Soc.* **2004**, *126*, 13550–13559. [[CrossRef](#)]
49. Bisquert, J.; Zaban, A.; Salvador, P. Analysis of the Mechanisms of Electron Recombination in Nanoporous TiO₂ Dye-Sensitized Solar Cells. Nonequilibrium Steady-State Statistics and Interfacial Electron Transfer via Surface States. *J. Phys. Chem. B* **2002**, *106*, 8774–8782. [[CrossRef](#)]
50. Fabregat-Santiago, F.; Garcia-Belmonte, G.; Mora-Seró, I.; Bisquert, J. Characterization of Nanostructured Hybrid and Organic Solar Cells by Impedance Spectroscopy. *Phys. Chem. Chem. Phys.* **2011**, *13*, 9083–9118. [[CrossRef](#)]
51. Bisquert, J.; Fabregat-santiago, F.; Mora-Seró, I.; Garcia-Belmonte, G.; Giménez, S. Electron Lifetime in Dye-Sensitized Solar Cells: Theory and Interpretation of Measurements. *J. Phys. Chem. C* **2009**, *113*, 17278–17290. [[CrossRef](#)]
52. Nazeeruddin, M.K.; Humphry-Baker, R.; Liska, P.; Grätzel, M. Investigation of Sensitizer Adsorption and the Influence of Protons on Current and Voltage of a Dye-Sensitized Nanocrystalline TiO₂ Solar Cell. *J. Phys. Chem. B* **2003**, *107*, 8981–8987. [[CrossRef](#)]

Disclaimer/Publisher’s Note: The statements, opinions and data contained in all publications are solely those of the individual author(s) and contributor(s) and not of MDPI and/or the editor(s). MDPI and/or the editor(s) disclaim responsibility for any injury to people or property resulting from any ideas, methods, instructions or products referred to in the content.